Spring 4-5-2012

Electron Energy Dependent Charging Effects of Multilayered Dielectric Materials

Gregory Wilson
Utah State University

JR Dennison
Utah State University

Amberly Evans Jensen
Utah State University

Justin Dekany
Utah State University

Electron Energy Dependent Charging Effects of Multilayered Dielectric Materials

UtahStateUniversity MATERIALS PHYSICS GROUP

USU Materials Physics Group

Gregory Wilson, JR Dennison, Amberly Evans and Justin Dekany

Utah State University, Logan, Utah 84322-4415

Phone: (859) 559-3302, FAX: (435) 797-2492, E-mail: GregDWilson@gmail.com

12th Spacecraft Charging Technology Conference 14-18 May, 2012 Kitakyushu, Japan

Abstract

Measurements of the charge distribution in electron-bombarded, thin-film, multilayered dielectric samples showed that charging of multilayered materials evolves with time and is highly dependent on incident energy; this is driven by electron penetration depth, electron emission and material conductivity. Based on the net surface potential's dependence on beam current, electron range, electron emission and conductivity, measurements of the surface potential, displacement current and beam energy allow the charge distribution to be inferred. To take these measurements, a thin-film disordered SiO_2 structure with a conductive middle layer was charged using 200 eV and 5 keV electron beams with regular 15 s pulses at 1 nA/cm² to 500 nA/cm². Results show that there are two basic charging scenarios which are consistent with simple charging models; these are analyzed using independent determinations of the material's electron range, yields, and conductivity. Large negative net surface potentials led to electrostatic breakdown and large visible arcs, which have been observed to lead to detrimental spacecraft charging effects.

Experimentation

In order to investigate the charging of multilayered dielectric materials, pulsed charging experiments were conducted using multilayered dielectric materials of an SiO_2 based optical coating, a conductive middle layer and an SiO_2 substrate. Tests were made with the conductive layer both grounded and ungrounded. Experiments were conducted in the main USU electron emission ultrahigh vacuum test chamber, modified for observations of low intensity UV/VIS/NIR glow over a broad range of sample temperatures. Figure 1 provides a general schematic of the experimental system used.

The samples were subjected to short pulses (t_{on}≈15 s) of electron bombardment using a monoenergetic electron beam with beam energies of either 200 eV or 5 keV. A low energy electron gun [Staib, EK-5-S1] was used, that can deliver a well-characterized, low-flux pulsed beam (typically ~50pA/cm² to 1 μA/cm²) over an energy range of 20 eV to 5 keV. The defocused electron beam produced a beam profile at the sample with about ±30% uniformity over an ~3 cm diameter beam spot. Beam fluxes were monitored with a Faraday cup. Beam current densities of 20±1 nA/cm² at 200 eV and 2.7±1 nA/cm² at 5 keV were used for the experiments reported here, with an exposed sample area of 4.9±0.2 cm².

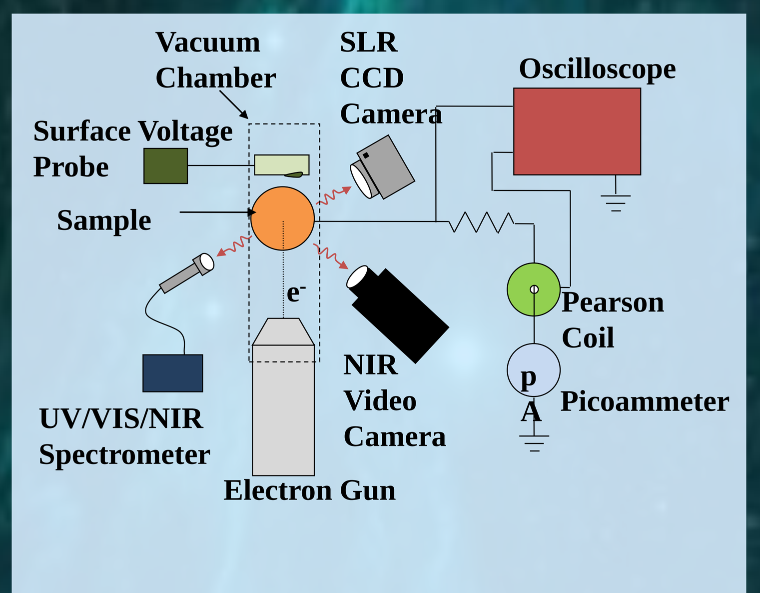

Fig. 1. Block diagram of instrumentation for collecting the pulse charging surface voltage and electrode current data induced by electron beam bombardment. Instrumentation includes picoammeters, Pearson coils, and a storage oscilloscope for electrode current measurements and UV/VIS and IR spectrometers, an SLR CCD still camera, and a NIR video camera for optical measurements.

Theory

Four experiments are considered as depicted in Fig. 6. The experiments differ in terms of the incident energy and flux, and as we will see below, produce dramatically different results. To interpret the experiments, we must consider three physical phenomena—the electron range, electron yield and the electron transport (conductivity) of the material—and how they are affected by the experimental conditions.

Range

The electron range is the maximum distance an electron of a given incident energy can penetrate through a material at a given incident energy, E_b, as the incident electron undergoes a succession of energy loss collisions and ultimately deposits charge at $R(E_b)$ when all energy is expended (see Fig. 4). Figure 2(a) shows the results of a composite model for the energy dependence of the range spanning from a few eV to 10^7 eV. Knowing the range of electrons becomes especially critical when dealing with multilayered materials, where the incident energy will determine where and in what layer charge and energy are deposited. The low (200 eV) and high (5 keV) incident energies were selected for these experiments based on range calculations to deposit charge at the mid-point between the surface dielectric and the conductor and into the conductive layer, respectively

Electron Yield

The total electron yield is defined as the ratio of emitted to incident flux and is highly energy dependent. The incident flux is the total number of electrons entering the material from the environment; the emitted flux is the sum of backscattered and secondary electrons, as shown in Fig. 4. Secondary electrons generally have energies <50 eV, while backscattered electrons generally have energies >50 eV.

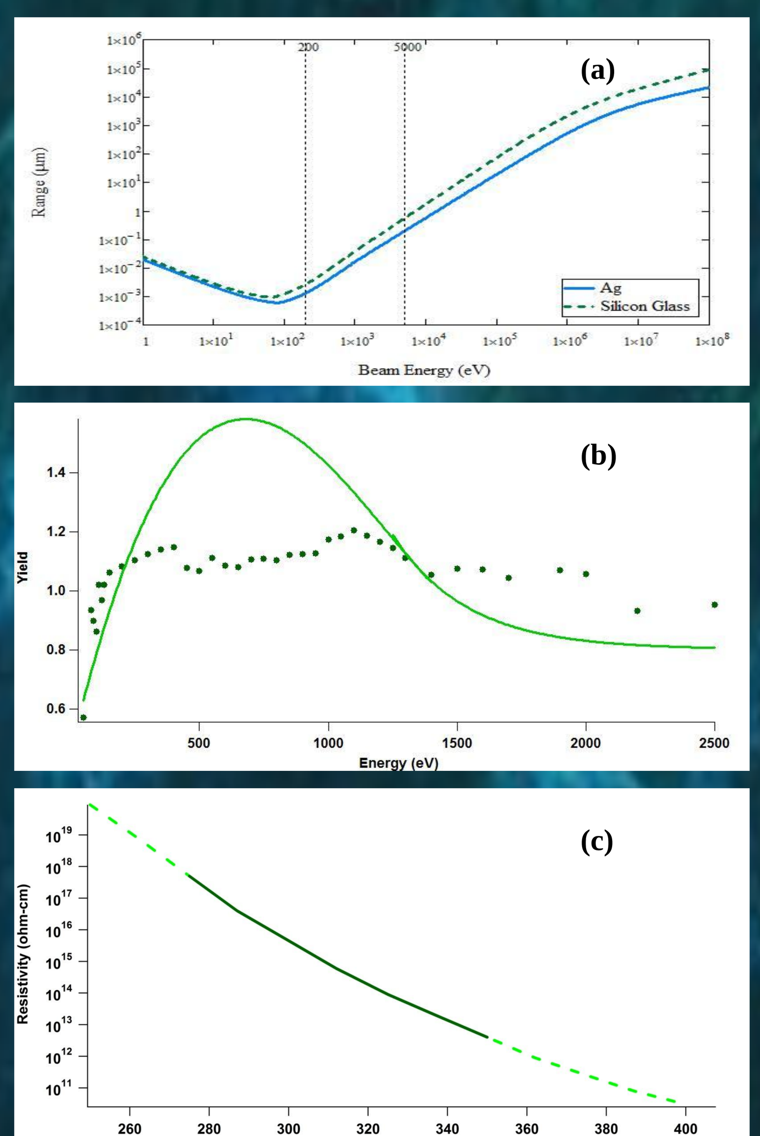

Fig. 2. (a) Range $R(E_b)$ as a function of incident energy for Ag and for SiO_2. (b) Total Electron yield as a function of incident energy for SiO_2. (c) Resistivity as a function of temperature for SiO_2.

Backscattered electrons undergo a quasi-elastic collision near the surface and backscatter, imparting no net charge to the material. Secondary electrons are generated by incident electrons that undergo collisions near the surface, which impart energy to several other electrons in the material. Some of these other electrons then escape the material's surface leading to net charge loss. The total yield is the sum of the backscattered yield and the secondary yield. When the total yield is less than unity, charging is negative. When the total yield exceeds unity, the material's surface becomes positively charged. As the net surface potential reaches a potential of a few volts positive, some secondary electrons are re-attracted to the surface which then can recombine with electron holes creating an upper limit on the net surface potential.

Conductivity

The conductivity of a material determines how easily a deposited charge layer can move through the material in response to an electric field. These electric fields, F, are produced by the embedded charge layers, the depletion layer, and the conductive planes in the material as modeled in Figs. 5 and 6. The measured currents will have two terms, a particle current conductivity proportional to the conductivity and a displacement current due to the change in the electric field due to charge accumulation.

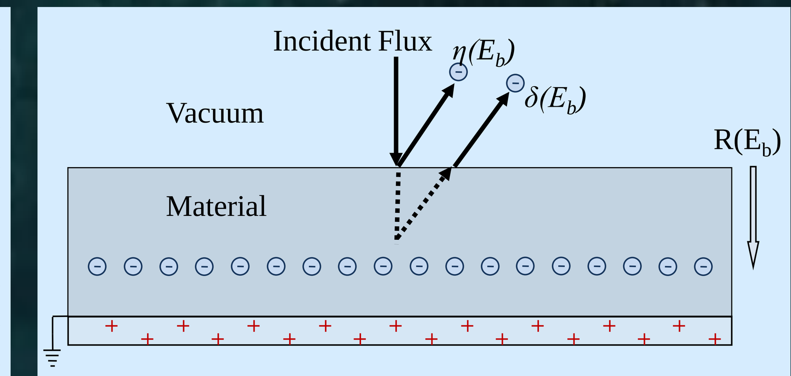

Fig. 4. Diagram of incident electron flux impinging on a generic material. $\eta(E_b)$ denotes the backscattered yield while $\delta(E_b)$ denotes the secondary yield. The total yield for all emission energies is the sum $Y(E_b)= \eta(E_b)+ \delta(E_b)$.

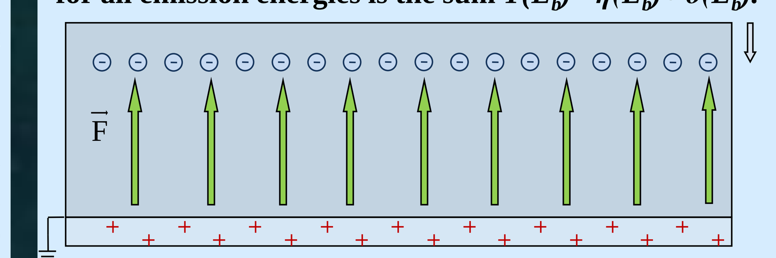

Fig. 5. Electric fields arise due to embedded charge layer(s) and grounded planes. The resulting electric field can lead to charge transport of the embedded charge layer and displacement currents resulting from charge migration to the grounded planes. Conductivity determines how fast embedded charges can move.

Models

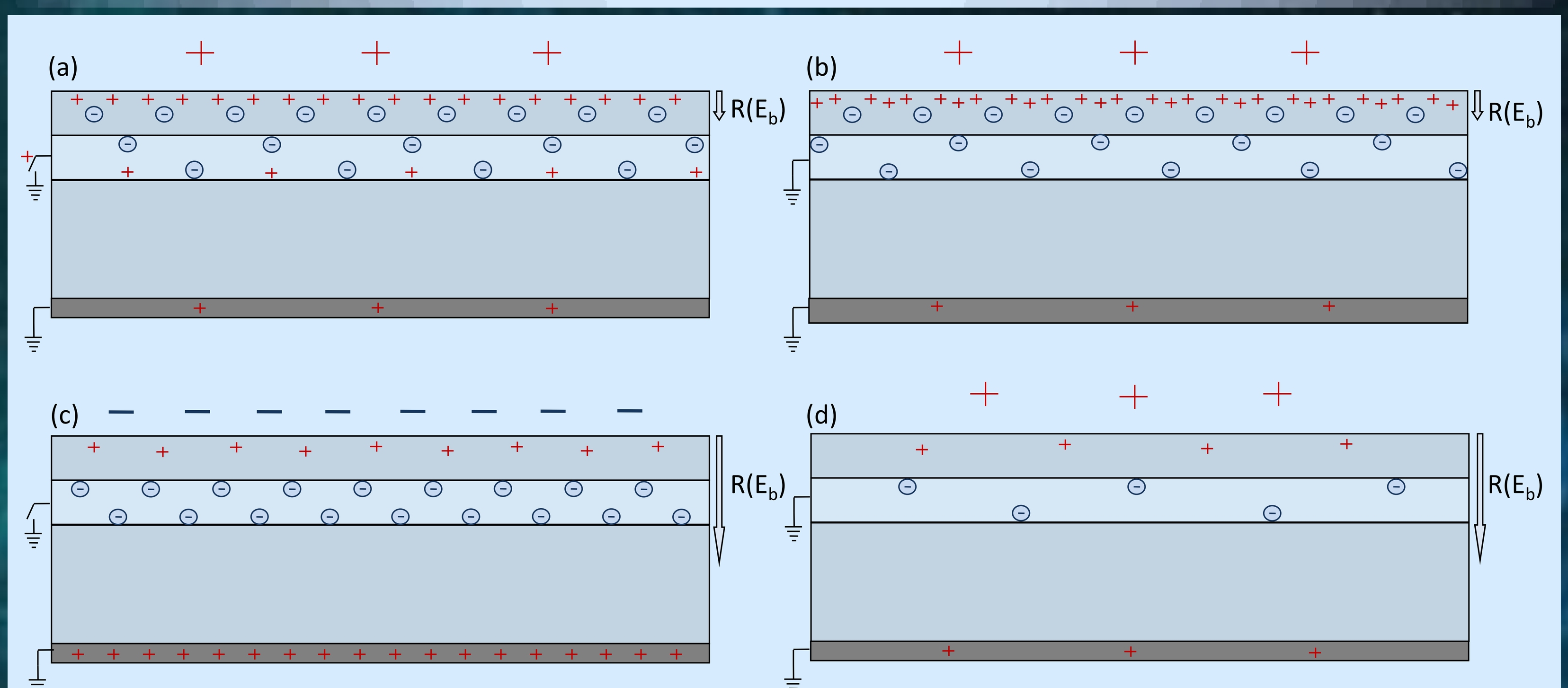

Fig. 6. Charging models for a multilayered dielectric with a conducting substrate: (a) surface dielectric deposition with low energy electron beam and ungrounded conductive layer, (b) surface dielectric deposition with low energy electron beam and grounded conductive layer, (c) conductive layer deposition with high energy electron beam and ungrounded conductive layer, (d) conductive layer deposition with high energy electron beam and grounded conductive layer. Electrons are shown as blue circles ⊖ and positive charge centers (holes) are shown as red +. Positive (a, b, d) and negative (c) surface voltages are indicated.

Surface Dielectric Deposition—Ungrounded

For a 200 eV monoenergetic electron beam the electron range in disordered SiO_2 is approximately 3 nm, as shown in Fig. 2(a). At this depth, the electrons just penetrate into the first layer, but do not reach the conductive layer. From Fig. 2(b) the total yield for disordered SiO_2 at this energy is >1, which leads to a positive charge depletion layer. Thus, we should see a self-limiting positive net surface potential due to a net deficit of electrons; this agrees with the sign of the measured net surface potential as measured in Fig. 7(a).

Surface Dielectric Deposition—Grounded

For a 200 eV electron beam with a grounded conductive layer, we expect similar behavior for the surface voltage as seen for the ungrounded scenario. Positive surface voltage is observed in Fig. 7(c), as expected.

Conductive Layer Deposition—Grounded

For a 5 keV monoenergetic electron beam the electron range in disordered SiO_2 is ~560 nm, as shown in Fig. 2(a). At this depth, the electrons penetrate through the surface dielectric and into the conductive layer. The total yield for disordered SiO_2 at this energy is <1, which should lead to a negative net surface potential in Fig. 7(g). However, because the conductive layer is grounded, charge will dissipate quickly from the conductive layer. Although the electron yield is <1 for a 5 keV electron beam, there will still be a positively charged deficit layer near the surface which will behave similar to the low energy scenarios, thus we should observe a self-limiting small positive potential similar to Fig. 7(a)., which is confirmed in Fig. 7(g).

Conductive Layer Deposition—Ungrounded

For a 5 keV electron beam with an ungrounded conductive layer, we again deposit charge in the conductive layer. We also have a total electron yield less than unity as before. Because the conductive layer is ungrounded there will be no fast charge dissipation mechanism. Thus, because there is no limiting behavior from re-attraction of secondary electrons, we should see a high net negative potential. This is confirmed in Fig. 7(e). For this scenario, after higher negative net surface potentials were reached, breakdown and arcing was observed.

ACKNOWLEDGEMENT

We gratefully acknowledge contributions to instrumentation and experimental efforts from Josh Hodges, Robert Johnson, and Doug Ball of the Materials Physics Group, Michael Taylor for the use of infrared and CCD video cameras, aid with theoretical models from Alec Sim, and useful discussions with Robert Meloy and Charles Bowers of NASA Goddard Space Flight Center.

Results

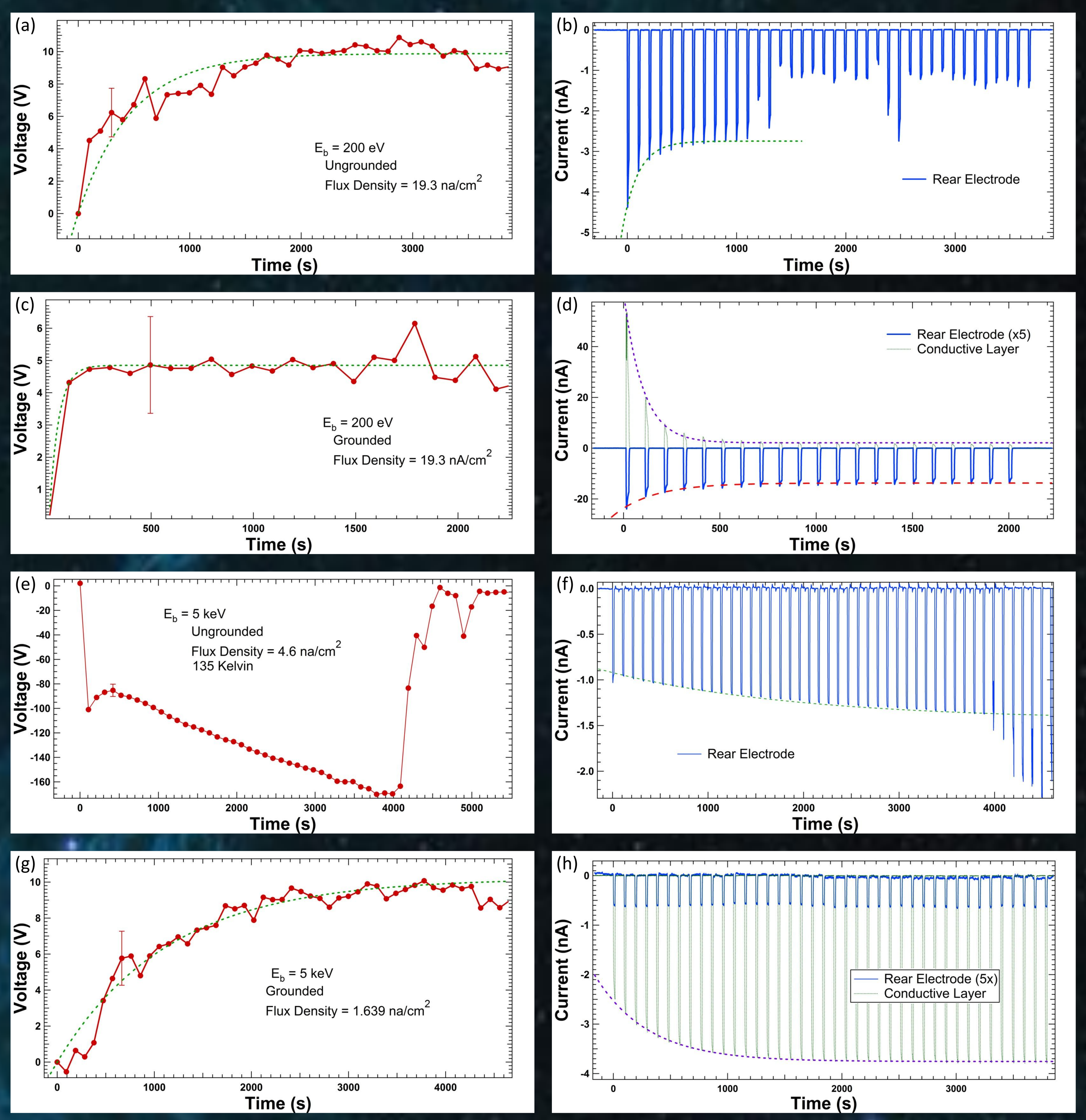

Fig. 7. Measurements of surface potentials vs time (a, c, e, g) and rear electrode and conductive layer currents vs time (b, d, f, h) for: (a, b) surface dielectric deposition with low energy electron beam and ungrounded conductive layer; (c, d) surface dielectric deposition with low energy electron beam and grounded conductive layer; (e, f) dielectric substrate deposition with high energy electron beam and ungrounded conductive layer; and (g, h) dielectric substrate deposition with high energy electron beam and grounded conductive layer. (a,b,c,d,g,h) were done at 298 K with (e,f) at 135 K. Exponential fits for the voltage was based on Eq. 3 with (a) τ=475 s (τ_Q =6.6 μC), (c) τ=45 s (τ_Q =0.63 μC), (g) τ=1137 s (τ_Q =1.33 μC). Exponential fits for the currents were based on Eq. 5 with (b) τ=139 s (τ_Q =1.93 μC), (d) conductive layer τ=99 s (τ_Q =1.37 μC), rear electrode τ=206 s (τ_Q =2.86 μC) (f) τ=2880 s (τ_Q =3.37 μC), (h) τ=462 (τ_Q =0.54 μC).

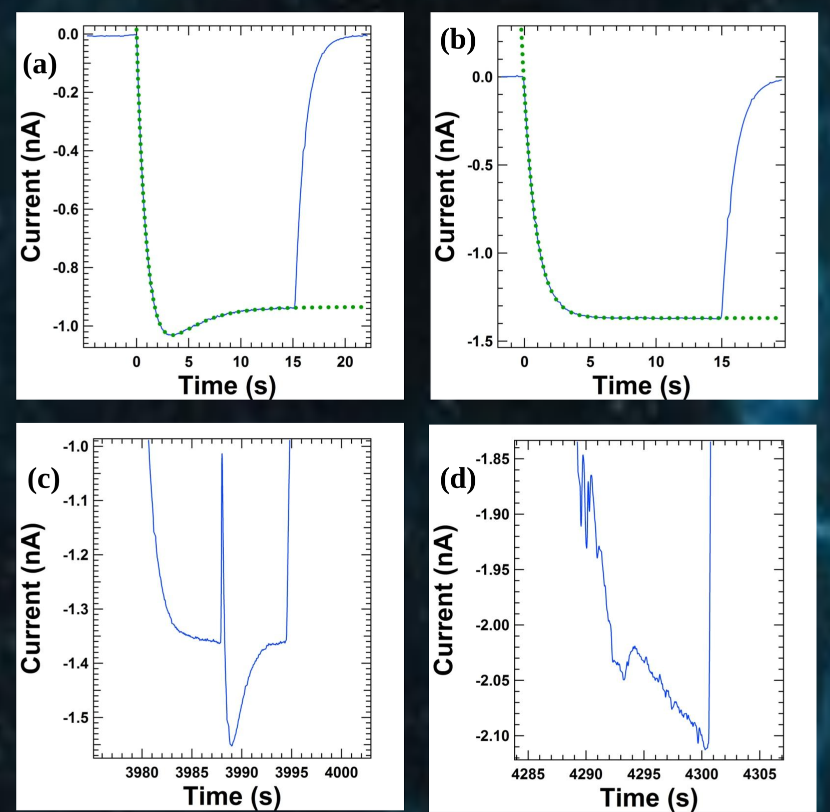

Fig. 8. Expanded views of the rear electrode current in Fig. 7(f) . (a) First current pulse τ_{Disp} = 0.507 ± 0.008 s (4.0 ± 0.06 nC) and 1.444 ± τ_Q = 0.007 (11.3 ± 0.06 μC). (b) Current pulse immediately before the first observed arc τ_Q = 0.966 ± 0.001 s (7.53 ± 0.007 nC) (c) Current during first arc. (d) Current after subsequent arcing.

<u>Surface Voltage</u>

Once an insulator with a grounded backplane is exposed to an electron flux, to first order, the surface potential charges according to the capacitance model

$$V_S(t) = V_{inj}(t)\left(1 - e^{-\frac{t\sigma(t)}{\varepsilon_0\varepsilon_r}}\right) \quad (1)$$

where ε_0 is permittivity of free space, ε_r is the relative permittivity of the material, and V_0, the long term equilibrium,

$$V_0 = \frac{\bar{J}_0}{\sigma_o}[D - R(E_b)] \quad (2)$$

For the experiments here, $\left[\sigma(t)/\varepsilon_0\varepsilon_r\right] \ll t$ and the exponential term in Eq. (4) can be neglected. To account for the charge dependant electron emission given by Eq. (1), we write the injection voltage as [S]

$$V_{inj}(t) = V_o(t)[1 - Y(E_b)]\left(1 - e^{-Q(t)/\tau_Q}\right) \quad (3)$$

Fits for Fig. 7(a,c,f) are based on these exponential modes with their corresponding parameters reported.

<u>Electrode Current</u>

The current measured at the grounded rear electrode includes two contributions, the free charge transport current density, J_c, and the charge displacement current density, $J_{displacement}$.

$$J_{elec}(t) = J^c_{elec}(t) + J^{displacement}_{elect} = \sigma(t)F(t) + \epsilon_o\epsilon_r\frac{\partial F(t)}{\partial t} \quad (4)$$

For the time independent conductivity estimated above and for general voltage expressions for the parallel plate geometry, it can be shown that this current is given by

$$J(t) = \bar{J}_0(t)[1 - Y(E_b)]\left(1 - e^{-Q(t)/\tau_Q}\right)\left\{1 + \left[1 + {}^{\tau_d}/_{t_{on}}\right]^{-1}\right\} \quad (5)$$

Fits based on these models, with the displacement current neglected due to long time frames, are shown in Fig 7(a,d,f,h) with their respected values reported. Figure 8(a,b) also have fits based on these models but (a) also includes an exponential for the displacement current. After several beam pulses the displacement current dies out as shown in Fig. 8(b).